[Article] doi: 10.3866/PKU.WHXB201702093 www.whxb.pku.edu.cn

不同生物炭材料的制备及其在Li-S电池中的应用

李君涛[1,*] 吴娇红[1] 张 涛[1] 黄 令[2]
([1]厦门大学能源学院，福建 厦门 361005；[2]厦门大学化学化工学院，福建 厦门 361005)

摘要：通过可再生生物质制备的生物炭具有成本低、环保和资源可再生的优势。本研究以分布广泛的稻谷壳、芒草、杉木和柚子皮等生物质为原料，制备了4种不同类型生物炭，然后研究了其作为锂-硫电池硫/碳正极的载体的性能。研究表明由稻谷壳制备的硫/生物炭正极材料表现出最高的比容量和最优的循环稳定性。为了进一步改善其电性能，以SiO_2溶胶为模板制备了具有高孔隙率的稻谷壳生物炭，其多孔结构可有效抑制多硫化物的溶解。由此得到的硫/生物炭(硫含量为60% (*w*，质量分数))材料中的硫以无定型态均匀地分散在碳载体中。该材料表现出更优异的电化学性能：在0.2*C* (1*C* = 1675 mA·g^{-1})倍率下，首周放电容量为1534.1 mAh·g^{-1}，循环100周后仍可保持在783.7 mAh·g^{-1}；倍率性能测试中，在2.0*C*倍率下，材料的可逆容量为485.3 mAh·g^{-1}。

关键词：锂硫电池；复合物；稻壳；芒草；杉木；柚子皮
中图分类号：O646.21

Preparation of Biochar from Different Biomasses and Their Application in the Li-S Battery

LI Jun-Tao[1,*] WU Jiao-Hong[1] ZHANG Tao[1] HUANG Ling[2]
([1]*College of Energy, Xiamen University, Xiamen 361005, Fujian Province, P. R. China*;
[2]*College of Chemistry and Chemical Engineering, Xiamen University, Xiamen 361005, Fujian Province, P. R. China*)

Abstract: Biochar derived from reproducible massive biomasses presents the advantages of low cost and renewable resources. In this work aiming to solve the existing problems of the lithium-sulfur battery, sulfur@biochar (S@biochar) composite cathode materials with high capacity and good cycle performance were developed. Specifically, four kinds of biochar prepared from rice husk, miscanthus, fir, and pomelo peel were used as host matrices for the Li-S battery. Among them, the S@biochar derived from rice husk delivered the highest specific capacity and the best cycle stability according to electrochemical tests. To further optimize its performance, we prepared a highly porous rice husk derived biochar (HPRH-biochar) using silica gel as the template. The S@HPRH-biochar composite (60% (*w*, mass fraction) S) enables the homogeneous dispersion of amorphous sulfur in the carbon matrix and its porous structure could effectively suppress the dissolution of the polysulfide. As a result, its electrochemical performance improved, achieving a high initial charge capacity of 1534.1 mAh·g^{-1} and maintaining a high capacity of 738.7 mAh·g^{-1} after 100 cycles at 0.2*C* (1*C* corresponds to a current density of 1675 mA·g^{-1}). It also gives a capacity of 485.3 mAh·g^{-1} at 2.0*C* in the rate capacity test.

Key Words: Li/S battery; Composite; Rice husk; Miscanthus; Fir; Pomelo peel

Received: December 28, 2016; Revised: February 3, 2017; Published online: February 9, 2017.
*Corresponding author. Email: jtli@xmu.edu.cn; Tel: +86-592-5197067.
The project was supported by the National Natural Science Foundation of China (21373008) and Fundamental Research Funds for the Central Universities, China (20720160124).
国家自然科学基金(21373008)和中央高校基本科研业务费(20720160124)资助项目

1 Introduction

Due to the impending energy and environmental issues, rechargeable electrochemical batteries with high energy density and long cycle ability are in high demand. The lithium-sulfur (Li-S) battery is one of the most potential solutions due to its high theoretical capacity (1675 $mAh \cdot g^{-1}$ for Li_2S). Moreover, sulfur, due to the advantages of low cost, natural abundance and environmental friendliness, has been an attractive cathode candidate material for a large-scale practical application. Nevertheless, there still remains three major problems to be settled, which includes: (1) the inherently poor electrical conductivity of elemental sulfur (5×10^{-30} $S \cdot cm^{-1}$ at 25 °C); (2) the dissolution and shuttling problems with the lithium polysulfide intermediates in non-aqueous electrolyte; and (3) the volume expansion/contraction of sulfur during the electrochemical cycling. All of the above issues could cause rapid capacity decay and low coulombic efficiency of Li-S battery[1−4].

To overcome these challenges, considerable efforts have been carried out on exploring new battery configuration[5], additives[6,7], novel organic electrolytes[8,9], polymer/sulfur composites[10], and sulfur/carbon composites[11−16]. Recently, various porous carbon materials such as porous carbon nanofibers[11], carbon nanotubes[12], porous hollow carbon spheres[13], carbon fibers/nanofoam composite[14], metal organic framework (MOF)[15], and MOF-derived porous carbon[16] have been studied and proved to be one of the most promising methods to improve the electrochemical performances of Li-S batteries, as the porous carbon can both serve as a host to trap sulfur and provide conductive paths to facilitate electron migration. However, most of these porous carbon materials are either expensive or require complex synthesis processes, which makes them difficult to scale up for practical application in the Li-S battery systems.

In the last few years, reproducible massive biomasses with low cost have attracted great attention due to their potential application in the preparation of carbon materials. Biomass such as banana fibers[17], peanut shells[18], cherry stones[19], sugar[20], coffee shells[21], alginic acid fiber[22], silk cocoon[23] and rice husk[24,25] have been served as carbon sources and showed many excellent features. Zhang *et al*. had successfully prepared porous carbons with high surface area from rice straw, which showed an excellent reversible capacity for anode materials in lithium-ion batteries[26]. In case of Li-S battery, the biochar materials are promising host matrixes for encapsulating sulfur, which enables efficient electrical contact between the conductive carbon framework material and sulfur. The porous carbon/sulfur composite with hierarchically porous structure was prepared from silk cocoon by the thermal carbonization with KOH[23]. This electrode material showed a high initial discharge capacity of 1443.0 $mAh \cdot g^{-1}$ and a capacity of 804.0 $mAh \cdot g^{-1}$ could be retained after 80 discharge/charge cycles at 0.5*C*. In addition, a kind of 3D structured carbon material was prepared from pomelo peel[27]. After a solution infiltration method with sulfur, the resulting sulfur/activated carbon foam nanocomposite showed an initial discharge capacity of 1258 $mAh \cdot g^{-1}$ at 0.2*C*, with a capacity of 750 $mAh \cdot g^{-1}$ retained after 100 cycles. Tao *et al*.[28] also used the Kapok fiber derived carbon nanotiles as the host of sulfur. The as-prepared composite electrodes showed a high and stable capacity of 524 $mAh \cdot g^{-1}$ after 90 cycles at 0.4 $A \cdot g^{-1}$. Moreno *et al*. used activated carbon derived from olive stones for the matrix in the S/C composites[29], and the resulting cathode possessed a high capacity of about 670 $mAh \cdot g^{-1}$ after 50 cycles and a good rate capability. On the basis of the above review, it could be noticed that the biochar derived from different biomasses would possess different structural and even compositional features, which thus lead to distinct electrochemical performances for the relevant biochar/sulfur cathode. To promote their applications in Li-S battery, it is still necessary to compare and optimize the properties of different kinds of biochar.

Among innumerable species of biomasses, the rice husk (RH), miscanthus (M), fir (F), and pomelo peel (PP) are the most popular and readily available ones whose estimated worldwide productions are as large as million tons. The rational utilization of such massive biomasses would make great sense. In this study, the applications of four kinds of different biochar which is respectively derived from rice husk, miscanthus, fir, and pomelo peel are explored and compared in Li-S battery for the first time. What′s more, silica template was introduced in the preparation of rice husk derived biochar, and a highly porous rice husk derived biochar was produced accordingly, which brings enhanced performance for the resulting sulfur/biochar cathode.

2 Experimental

2.1 Materials synthesis

The biochar from different biomasses was prepared as follows. The raw biomasses including rice husk, miscanthus, fir, and pomelo peel were milled and washed by deionized water to remove the impurities on the surface, and dried at 100 °C for 24 h. Then thermal carbonization of the biomasses was carried out at 800 °C for 2 h with a heating rate of 5 $°C \cdot min^{-1}$ under Ar gas in a tubular furnace. Afterward, the black residues were immersed in a mixed solution with 1 $mol \cdot L^{-1}$ HCl (AR) and 10% (*w*, mass fraction) HF (AR) under vigorous magnetic stirring overnight to remove silica and other soluble minerals in the pristine biomass. After washing with deionized water and ethanol (AR) for several times, the as-prepared biochar was dried at 80 °C in a vacuum oven overnight.

To optimize the biochar from rice husk, colloidal silica (Aldrich, 40% (*w*) SiO_2) was used as hard template to prepare the highly porous rice husk biochar. Typically, rice husk (5 g) and silica sol (10 g) were well dispersed in water through ultrasonic treatment. Subsequently, the water was evaporated at 80 °C under vigorous magnetic stirring. Then the resulting powder was calcined at 800 °C for 2 h with a heating rate of 5 $°C \cdot min^{-1}$ under Ar atmosphere in a tubular furnace. Afterward, the residue was treated by 1 $mol \cdot L^{-1}$ HF solution to remove the silica template. Thus prepared highly porous rice husk derived biochar after being washed several times with deionized water, was dried at 80 °C.

As to the preparation of the S@biochar composite, the biochar and sulfur mixture with different mass ratios, after being ground sufficiently in an agate mortar, was transferred to a 50 mL Teflon-lined autoclave and maintained at 155 °C for 12 h. NETZSCH STA 449 F5 analyzer was used to thermal gravimetric measure the sulfur content in S@biochar composites.

2.2 Structure characterization

The as-prepared porous carbon and S@biochar composite were characterized by X-ray diffraction (XRD, Panalytical X′pert PRO, Philip). The morphology and the structure of the samples were characterized by field emission scanning electron microscopy (SEM, S-4800, Hitachi), transmission electron microscopy (TEM, JEM 2100, JEOL). The specific surface area was measured by BET N_2 sorption isotherms (Micromeritics Tristar 3000).

2.3 Electrochemical measurement

The working electrodes were made from active materials (S@biochar composite), conductive agent (BP2000) and binder (poly(vinylidene difluoride) (PVDF) (AR)) with *N*-methy-2-pyrrolidone (NMP) (AR) as dispersant with a mass ratio of 70 : 20 : 10. After forming a homogeneous slurry *via* magnetic stirring, the mixture was spread on Al foils using a doctor-blade coating method and was then heated in a vacuum oven at 55 °C for 24 h. CR2025 coin-type cells were assembled in a glove box filled with Ar. Li foil was used as the counter electrode and the Celgard 2400 as the separator. The electrolyte was 1 mol·L^{-1} bis-(trifluoromethane) sulfonimide lithium (LiTFSI, Alfa Corp.) and 0.1 mol·L^{-1} lithium nitrate ($LiNO_3$) in dimethoxyethane (DME) and 1,3-dioxolane (DOL) (1 : 1 (*V*/*V*)) (Fosai New Materials Co., Ltd., JiangSu, China). The electrochemical measurements were conducted on a LAND CT2001A instrument (Wuhan, China) at room temperature. The cells were discharged and charged in the fixed voltage range of 1.5−3.0 V (*vs* Li/Li^+). 1 *C* corresponds to a current density of 1675 mA·g^{-1}. Cyclic voltammetry (CV) measurements were performed on an electrochemistry working station CHI660D (Chenhua Co., Ltd., Shanghai, China) at a scanning rate of 0.2 mV·s^{-1}. Electrochemical impedance spectroscopy (EIS) was carried out between 100 kHz to 0.01 Hz on a VERSASTATV3 electrochemical workstation (Princeton Applied Research, USA). ZView software (Scribner, Inc.) was used to fit the EIS spectra.

3 Results and discussion

Fig.1 shows the morphologies of the resulting four kinds of the biochar. All of the four kinds of biochar are composed of large irregular particles with a diameter of 10−30 μm. Especially, the particles of the rice husk derived biochar (RH-biochar) exhibit a hierarchical pore structure, with numerous macro pores ranging from 1 to 10 μm easily identified under the SEM observation (Fig.1 (a)). Such a result clearly indicates that RH-biochar possesses high specific area. The particles of the biochar prepared from the miscanthus (M-biochar) (Fig.1(b)) also have some pores, though much less than that in the RH-biochar. The biochar samples from fir (F-biochar) (Fig.1(c)) and pomelo peel (PP-biochar) (Fig.1(d))

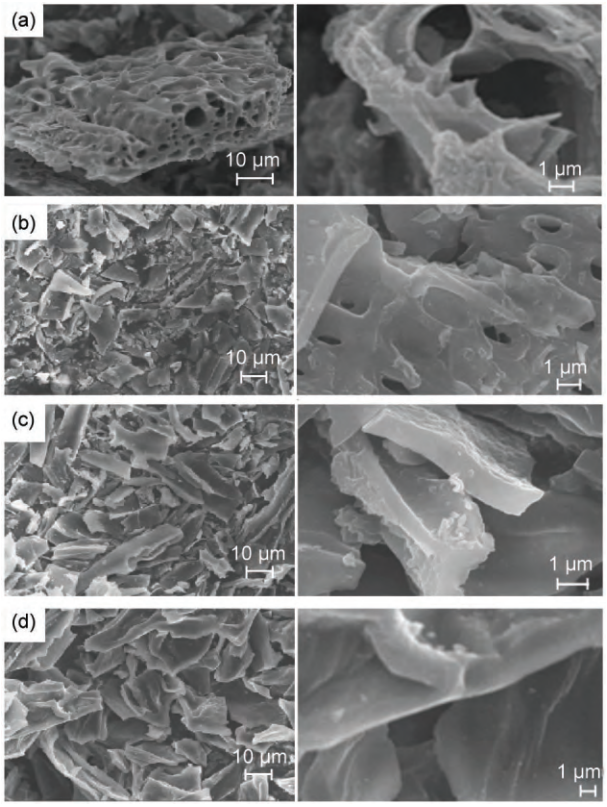

Fig.1 SEM images of biochar (with different resolutions) derived from (a) rice husk, (b) miscanthus, (c) fir, and (d) pomelo peel

show plate-like morphology with relative smooth surface, and no obvious pores can be revealed on such plate-like particles under SEM observation. BET analysis reveals that the specific surface areas of the biochar from rice husk, miscanthus, fir, and pomelo peel are 1075.3, 397.9, 622.7, and 638.1 $m^2 \cdot g^{-1}$, respectively, confirming the highest surface area of RH-biochar. Such comparative results clearly demonstrate that the morphologies and structures of the biochar are greatly affected by the species of the biomass sources. With such large surface area and hierarchical pore structures, one could expect that our RH-biochar could make an excellent candidate for the adsorption of sulfur and lithium polysulfide intermediates.

The XRD patterns of the four biochar samples are shown in Fig.2. All of the four samples display typical XRD patterns of the amorphous carbon. A broad diffraction peak at around 24° is observed, which is consistent with the (002) diffraction peak of graphitic carbon. The low peak intensity/background ratio and high peak broadening prove the amorphous nature of the resulting biochar, which may be related with the relative low calcination temperature.

With the above biochar as carriers, the S@biochar composite cathodes were prepared with our previously reported melt-diffusion method[30]. For comparison, the S content in these composites was controlled to be 50% (the thermal gravimetric analysis (TGA) was shown in Fig.2(e)). The electrochemical performances of these four S@biochar composite cathodes are shown in Fig.3 (a). One can see that the S@RH-biochar shows a high discharge

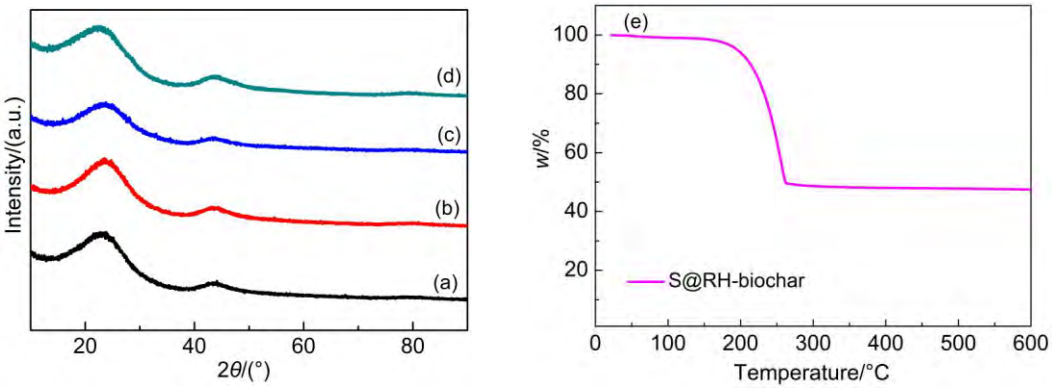

Fig.2 XRD patterns of biochar derived from (a) rice husk, (b) miscanthus, (c) fir, and (d) pomelo peel; (e) TGA curves of S@RH-biochar with 50% (*w*) S

capacity of 1005.5 mAh·g^{-1} at 0.2*C* with an initial Coulombic efficiency of 101.6%, which indicates that there is no obvious overcharge phenomenon. After 100 electrochemical cycles, 566.8 mAh·g^{-1} with a Coulombic efficiency of 96.9% could be retained, suggesting a high stability of this cathode. The S@biochar composites from miscanthus and pomelo peel give lower initial capacities, which are 824.5 and 892.8 mAh·g^{-1}, separately. And after 100 cycles, their capacity could be maintained at 388.2 and 393.8 mAh·g^{-1}, respectively. However, the initial Coulombic efficiency of S@biochar from pomelo peel is 110.7%, which could be associated with relatively severe shuttle effect. Though the S@biochar from fir displays the highest initial capacity of 1051.7 mAh·g^{-1}, its cycling stability is limited, which decays to only 532.5 mAh·g^{-1} after 100 cycles. What's more, the low initial Coulombic efficiency of 89.8% was observed on this cathode. Fig.3(b) is the discharge-charge curves of S@biochar cathodes at 0.2*C* in 1.5−3 V. Obviously, the S@RH-biochar cathode displays a longer voltage plateau than other S@biochar cathodes at the same electrode potential. On this basis, one could see that the S@RH-biochar delivered a superior electrochemical performance to those of the other three and we attribute its outstanding performance to its large specific surface area and its hierarchical pore structures. The electrochemical performances of different S@biochar cathodes are summarized in Table 1.

To further improve the electrochemical properties of the biochar derived from rice husk, silica template was introduced into its preparative process to create additional mesopores in the resulting biochar. The morphology and structure of thus-prepared biochar, namely the highly porous rice husk derived biochar (named as HPRH-biochar) are shown in Fig.4. The particle size of such HPRH-biochar is reduced compared with that derived with no addition of silica (i.e., the previously discussed RH-biochar). More

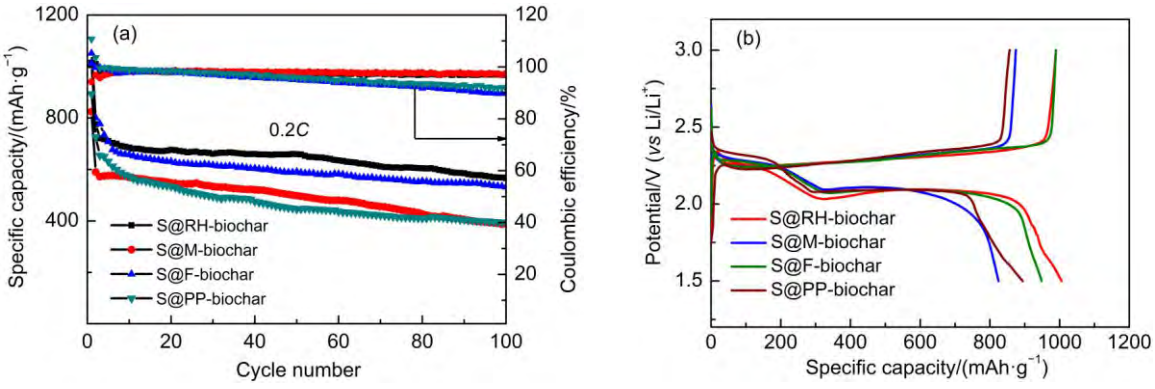

Fig.3 (a) Cycle performance and Coulombic efficiency and (b) charge-discharge profiles of S@RH-biochar, S@M-biochar, S@F-biochar and S@PP-biochar cathode in 1 mol·L^{-1} LiTFSI in DME and DOL (1 : 1 (*V*/*V*)) with 0.1 mol·L^{-1} $LiNO_3$ at 0.2*C*

The mass ratio of sulfur and biochar is 1 : 1.

Table 1 Summary of the electrochemical performance of S@biochar cathodes

S@biochar with 50% (*w*) S	Initial discharge capacity/(mAh·g^{-1})	Initial Coulombic efficiency/%	Discharge capacity after 100 cycles/(mAh·g^{-1})	Coulombic efficiency after 100 cycles/%
RH-biochar	1005.5	101.6	566.8	96.9
M-biochar	824.5	94.2	388.2	97.0
F-biochar	1051.7	101.4	532.5	89.8
PP-biochar	892.8	110.7	393.8	91.7

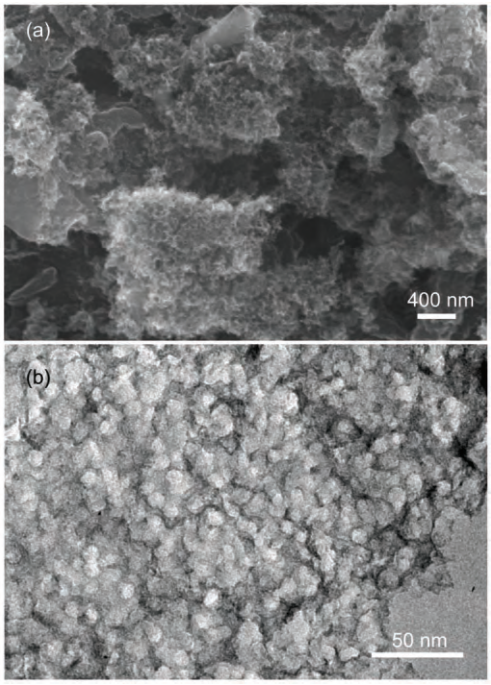

Fig.4 (a) SEM and (b) TEM images of the highly porous rice-husk-derived biochar (HPRH-biochar)

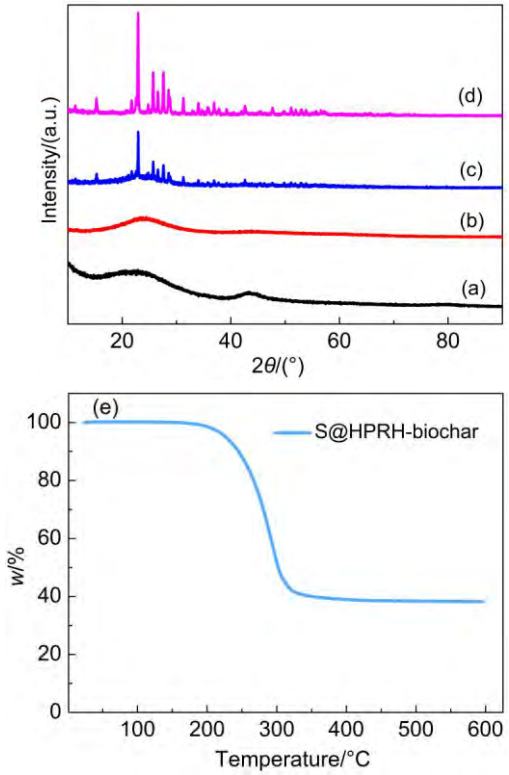

Fig.5 XRD patterns of (a) the pure HPRH-biochar, and the S@HPRH-biochar samples with (b) 60%, (c) 70%, and (d) 80% (*w*) S; (e) TGA curves of S@HPRH-biochar with 60% (*w*) S

importantly, massive mesopores with average size of 10 nm could be observed in the TEM image, which are generated using the silica colloidal particles as the template. The specific surface area of such HPRH-biochar is as large as 1960 $m^2 \cdot g^{-1}$, proving that the introduction of silica is an efficient strategy to improve the specific surface area of the biochar.

To determine the optimal S content, the S@HPRH-biochar samples with different S ratios were prepared with the melt diffusion method. The XRD patterns of the HPRH-biochar, namely the pure highly porous rice-husk-derived biochar, and the S@HPRH-biochar samples are shown in Fig.5. As can be seen, the original HPRH-biochar is amorphous in nature (Fig.5(a)). When the loading of S content is 60% (*w*) (the thermal gravimetric analysis was shown in Fig.5(e)), the composite remains amorphous according to its XRD pattern (Fig.5(b)), which indicates uniform dispersion of sulfur in the pores of the carbon. When the loading of S is further improved to, e.g., 70% (*w*) (Fig.5(c)) and 80% (*w*) (Fig.5(d)), peaks corresponding to bulk crystalline sulfur appear in their relevant XRD patterns, which is consistent with some previous reports[31].

Fig.6(a) shows the charge-discharge profiles of the S@HPRH-biochar with 60% (*w*) S in 1.5−3.0 V at 0.2*C*. A shorter potential plateau at about 2.3 V and longer potential plateau at 2.1 V are observed in the first discharge curve, which correspond to the reduction of sulfur to polysulfides and then to the Li_2S_2/Li_2S, respectively. In the first charge curve, a potential plateau at about 2.3 V is observed, owing to the transformation of sulfur species from Li_2S_x ($x > 2$). This voltage of potential plateau increases gradually in the following charge process. The CV curves of S@HPRH-biochar with 60% (*w*) S (Fig.6(b)) shows the presence of two reductive current peaks at about 2.0 and 2.3 V in the first cycle. These two peaks are positive-shifted in the following cycle. On a forward positive-going scan, an oxidative current peak at around 2.4 V is observed. The cycle performance and coulombic efficiency of S@RH-biochar and S@HPRH-biochar samples are compared in Fig.6(c). It can be seen that, for the S@RH-biochar cathode, the case loaded with 60% (*w*) S content shows higher initial charge capacity than that with a 50% (*w*) S content; however, the cycling stability of the former is inferior to the latter, with only 417.9 $mAh \cdot g^{-1}$ retained after 100 cycles test. It could be observed that the S@HPRH-biochar sample with an S loading of 60% (*w*) demonstrates a high initial charge capacity of 1534.1 $mAh \cdot g^{-1}$ and a capacity of 738.7 $mAh \cdot g^{-1}$ after 100 cycles, revealing an improved sulfur utilization, higher reversible capacity and better stability than the pristine biochar from rice husk. When the S content was further increased to 70% (*w*), the charge/discharge capacity of the S@HPRH-biochar cathode becomes even more stable in the first 100 cycles. As shown in Fig.6(c), an initial capacity of 1005.4 $mAh \cdot g^{-1}$ and 1299.7 $mAh \cdot g^{-1}$ could be obtained for the case with 70% (*w*) S and the one with 80% S, respectively, which decay to 569.0 and 486.2 $mAh \cdot g^{-1}$ after 100 cycles, correspondingly. Nevertheless, there are obvious capacity attenuations in sulfur@HPRH-biochar with the S of 70% and 80% (*w*) in the first several cycles. With increasing sulfur content, part of the sulfur would be located on the external surface of the carbon material due to the limitation of the pore volume of HPRH-biochar, which may lead to the dissolution of the polysulfide in the

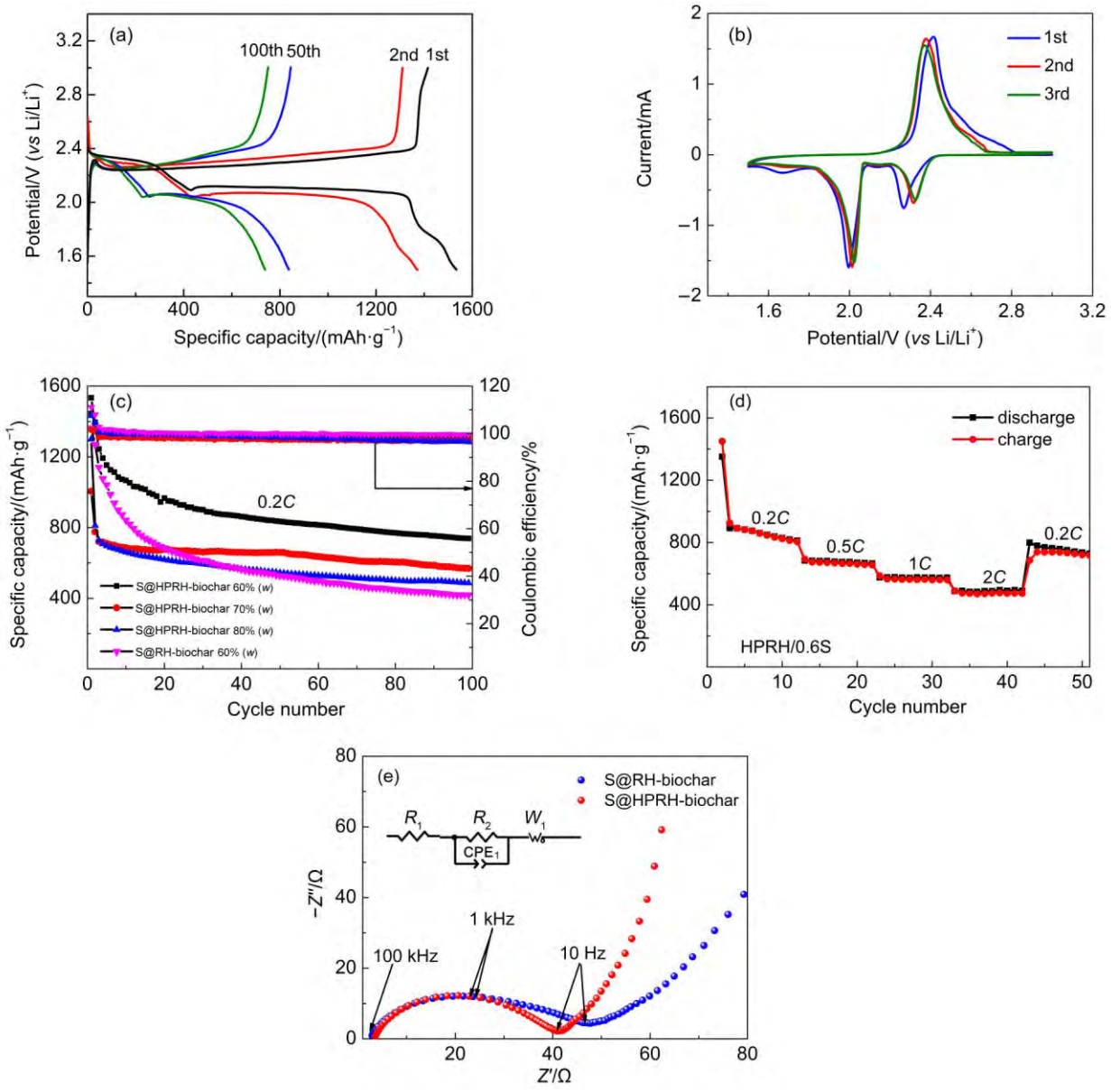

Fig.6 (a) Charge-discharge profiles and (b) cyclic voltammograms of S@HPRH-biochar (60% (*w*) S) cathode; (c) cycle performance and coulombic efficiency of S@RH-biochar (60% (*w*) S) cathode, and S@HPRH-biochar cathodes with 60%, 70%, and 80% (*w*) S at 0.2*C*; (d) rate capability of S@HPRH-biochar (60% (*w*) S) cathode; (e) EIS spectra of pristine S@RH-biochar (60% (*w*) S) cathode and S@HPRH-biochar (60% (*w*) S) cathode

The electrolyte is 1 mol·L^{-1} LiTFSI in DME and DOL (1 : 1, (*V*/*V*)) with 0.1 mol·L^{-1} $LiNO_3$. The inset is the equivalent circuit model. R_1 is the internal resistance of cell. R_2 and CPE_1 are the charge transfer reaction resistance and interface resistance, respectively. W_1 reflects the Warburg resistance.

electrolyte in the electrochemical cycle process, resulting in the loss of the active material form the electrode. The above results reflect the important effects of the S content on the electrochemical performances of the cathode. With significantly larger specific surface area, HPRH-biochar could accommodate more S content than the RH-biochar, which therefore results in evidently

Table 2 Comparison of the electrochemical performance of S@RH-biochar and S@HPRH-biochar cathodes with different S loading

S@biochar cathode	Initial discharge capacity/(mAh·g^{-1})	Initial coulombic efficiency/%	Discharge capacity after 100 cycles/(mAh·g^{-1})	Coulombic efficiency after 100 cycles/%
RH-biochar with 60% (*w*) S	1362.4	111.1	417.9	99.6
HPRH-biochar with 60% (*w*) S	1534.1	108.4	738.7	98.3
HPRH-biochar with 70% (*w*) S	1005.4	101.6	569.0	97.1
HPRH-biochar with 80% (*w*) S	1299.7	107.5	486.2	96.5

improved electrochemical performance. The electrochemical performances of S@RH-biochar and S@HPRH-biochar cathodes are compared in Table 2. The EIS spectra of pristine S@RH-biochar (60% (*w*) S) cathode and S@HPRH-biochar (60% (*w*) S) cathode are also compared in Fig.6(e). The S@HPRH-biochar cathode shows lower resistance value (36.1 Ω) than S@RH-biochar cathode (43.7 Ω). Various current rates were applied to evaluate the rate capability of S@HPRH-biochar composites with 60% (*w*) S. The rate performance illustrated in Fig.6(d) was conducted at 0.2*C*, 0.5C, 1.0*C*, 2.0*C*, and the reversible capacities are 870.2, 675.4, 571.8, 485.3 mAh·g^{-1}, respectively. When the current density turns back to 0.2*C*，a high capacity of 735.9 mAh·g^{-1} could be recovered. Such rate capability is comparable to the previous works[32−34].

4 Conclusions

In summary, four kinds of biochar derived from reproducible massive biomasses, including rice husk, miscanthus, fir, and pomelo peel, were prepared and explored as host matrixes materials to fabricate S@biochar composite cathodes of Li-S batteries. The S@biochar cathode derived from rice husk, owing to its hierarchical porous structure and high surface area, presents superior electrochemical performances to those from miscanthus, fir, and pomelo peel. Moreover, to further improve its performance, silica was introduced as the template to create massive mesopores, generating the highly porous rice husk biochar (HPRH-biochar) with evidently improved ability for accommodation of sulfur, and the S content was optimized. The S@HPRH-biochar with 60% (*w*) S shows the best performance, which achieves a high initial discharge capacity of 1534.1 mAh·g^{-1}, with a capacity of 738.7 mAh·g^{-1} retained after 100 cycles at 0.2*C*, and a rate capability of 485.3 mAh·g^{-1} at 2.0*C*. The research provides an efficient strategy for preparation of S@biochar cathode material with high energy density and excellent stability.

References

(1) Xin, S.; Gu, L.; Zhao, N. H.; Yin, Y. X.; Zhou, L. J.; Guo, Y. G.; Wan, L. J. *J. Am. Chem. Soc.* **2012,** *134*, 18510. doi: 10.1021/ja308170k

(2) Yang, Z.; Zhang, W.; Shen, Y.; Yuan, L. X.; Huang, Y. H. *Acta Phys. -Chim. Sin*. **2016,** *32*, 1062. [杨 泽, 张 旺, 沈 越, 袁利霞, 黄云辉. 物理化学学报, **2016,** *32*, 1062.] doi: 10.3866/PKU.WHXB201603231

(3) Ji, H. X.; Ruoff, R. S. *Acta Phys. -Chim. Sin.* **2016,** *32*, 797. [季恒星, Ruoff, Rodney S. 物理化学学报, **2016,** *32*, 797.] doi: 10.3866/PKU.WHXB201602192

(4) Yin, Y. X.; Xin, S; Guo, Y. G.; Wan, L. J. *Angew. Chem. Int. Edit*. **2013,** *52*, 13186. doi: 10.1002/anie.201304762

(5) Su, Y. S.; Manthiram, A. *Nat. Commun.* **2012,** *3*, 1166. doi: 10.1038/ncomms2163

(6) Lin, Z.; Liu, Z. C.; Fu, W. J.; Dudney, N. J.; Liang, C. D. *Adv. Funct. Mater.* **2013,** *23*, 1064. doi: 10.1002/adfm.201200696

(7) Zhang, S. S.; Read, J. A. *J. Power Sources* **2012,** *200*, 77. doi: 10.1016/j.jpowsour.2011.10.076

(8) Suo, L. M.; Hu, Y. S.; Li, H.; Armand, M.; Chen, L. Q. *Nat. Commun*. **2013,** *4*, 1481. doi: 10.1038/ncomms2513

(9) Jeddi, K.; Ghaznavi, M.; Chen, P. *J. Mater. Chem. A* **2013,** *1*, 2769. doi: 10.1039/c3ta01169k

(10) Wang, L.; He, X. M.; Li, J. J.; Chen, M.; Gao, J.; Jiang, C. Y. *Electrochim. Acta* **2012,** *72*, 114. doi: 10.1016/j.electacta.2012.04.005

(11) Zheng, G. Y.; Yang, Y.; Cha, J. J.; Hong, S. S.; Cui, Y. *Nano Lett*. **2011,** *11*, 4462. doi: 10.1021/nl304795g

(12) Guo, J. C.; Xu, Y. H.; Wang, C. S. *Nano Lett*. **2011,** *11*, 4288. doi: 10.1021/nl202297p

(13) Zhang, C. F.; Wu, H. B.; Yuan, C. Z.; Guo, Z. P.; Lou, X. W. *Angew. Chem. Int. Edit*. **2012,** *51*, 9592. doi: 10.1002/anie.201205292

(14) Chung, S. H.; Manthiram, A. *J. Mater. Chem. A* **2013,** *1*, 9590. doi: 10.1039/c3ta11819c

(15) Demir-Cakan, R.; Morcrette, M.; Nouar, F.; Davoisne, C.; Devic, T.; Gonbeau, D.; Dominko, R.; Serre, C.; Ferey, G.; Tarascon, J. M. *J. Am. Chem. Soc.* **2011,** *133*, 16154. doi: 10.1021/ja2062659

(16) Xi, K.; Cao, S.; Peng, X. Y.; Ducati, C.; Kumar, R. V.; Cheetham, A. K. *Chem. Commun*. **2013,** *49*, 2192. doi: 10.1039/c3cc38009b

(17) Stephan, A. M.; Kumar, T. P.; Ramesh, R.; Thomas, S.; Jeong, S. K.; Nahm, K. S. *Mater. Sci. Eng. A* **2006,** *430*, 132. doi: 10.1016/j.msea.2006.05.131

(18) Fey, G. T. K.; Lee, D. C.; Lin, Y. Y.; Kumar, T. P. *Synth. Met*. **2003,** *139*, 71. doi: 10.1016/S0379-6779(03)00082-1

(19) Arrebola, J. C.; Caballero, A.; Hernan, L.; Morales, J.; Olivares-Martin, M.; Gomez-Serrano, V. *J. Electrochem. Soc*. **2010,** *157*, A791. doi: 10.1149/1.3425728

(20) Xing, W.; Xue, J. S.; Dahn, J. R. *J. Electrochem. Soc*. **1996,** *143*, 3046. doi: 10.1149/1.1837162

(21) Hwang, Y. J.; Jeong, S. K.; Nahm, K. S.; Shin, J. S.; Stephan, A. M. *J. Phys. Chem. Solids* **2007,** *68*, 182. doi: 10.1016/j.jpcs.2006.10.007

(22) Wu, X. L.; Chen, L. L.; Xin, S.; Yin, Y. X.; Guo, Y. G.; Kong, Q. S.; Xia, Y. Z. *ChemSusChem* **2010,** *3*, 703. doi: 10.1002/cssc.201000035

(23) Zhang, B.; Xiao, M.; Wang, S. J.; Han, D. M.; Song, S. Q.; Chen, G. H.; Meng, Y. Z. *ACS Appl. Mater. Interface* **2014,** *6*, 13174. doi: 10.1021/am503069j

(24) Zhang, Y. C.; You, Y.; Xin, S.; Yin, Y. X.; Zhang, J.; Wang, P.; Zheng, X. S.; Cao, F. F.; Guo, Y. G. *Nano Energy* **2016,** *25*, 120. doi: 10.1016/j.nanoen.2016.04.043

(25) Fey, G. T. K.; Chen, C. L. *J. Power Sources* **2001,** *97−98*, 47. doi: 10.1016/S0378-7753(01)00504-3

(26) Zhang, F.; Wang, K. X.; Li, G. D.; Chen, J. S. *Electrochem. Commun.* **2009,** *11*, 130. doi: 10.1016/j.elecom.2008.10.041

(27) Zhang, J.; Xiang, J. Y.; Dong, Z. M.; Liu, Y.; Wu, Y. S.; Xu, C. M.; Du, G. H. *Electrochim. Acta* **2014,** *116*, 146. doi: 10.1016/j.electacta.2013.11.035

(28) Tao, X. Y.; Zhang, J. T.; Xia, Y.; Huang, H.; Du, J.; Xiao, H.; Zhang, W. K.; Gan, Y. P. *J. Mater. Chem. A* **2014,** *2*, 2290. doi: 10.1039/c3ta14113f

(29) Moreno, N.; Caballero, A.; Hernan, L.; Morales, J. *Carbon* **2014,** *70*, 241. doi: 10.1016/j.carbon.2014.01.002

(30) Li, X. L.; Cao, Y. L.; Qi, W.; Saraf, L. V.; Xiao, J.; Nie, Z. M.; Mietek, J.; Zhang, J. G.; Schwenzer, B.; Liu, J. *J. Mater. Chem*. **2011,** *21*, 16603. doi: 10.1039/c1jm12979a

(31) Chen, S. R.; Zhai, Y. P.; Xu, G. L.; Jiang, Y. X.; Zhao, D. Y.; Li, J. T.; Huang, L.; Sun, S. G. *Electrochim. Acta* **2011,** *56*, 9549. doi: 10.1016/j.electacta.2011.03.005

(32) Ye, X. M.; Ma, J.; Hu, Y. S.; Wei, H. Y.; Ye, F. F. *J. Mater. Chem. A* **2016,** *4*, 775. doi: 10.1039/c5ta08991c

(33) Tang, C.; Li, B. Q.; Zhang, Q.; Zhu, L.; Wang, H. F.; Shi, J. L.; Wei, F. *Adv. Funct. Mater.* **2016,** *26*, 577. doi: 10.1002/adfm.201503726

(34) Mi, K.; Jiang, Y.; Feng, J. K.; Qian, Y. T.; Xiong, S. L. *Adv. Funct. Mater.* **2016,** *26*, 1571. doi: 10.1002/adfm.201504835